



Trans. Nonferrous Met. Soc. China 34(2024) 1843-1863

Transactions of Nonferrous Metals Society of China

www.tnmsc.cn



Corrosion resistance of rapidly formed in-situ steam Mg-Al LDH coating on AM50 Mg alloy pretreated with oxalic acid

Shi-qi PAN 1 , Jin-meng WANG 1 , Fen ZHANG 1 , Hao-feng XIE 2 , Lan-yue CUI 1 , M. BOBBY KANNAN 3 , Yu-hong ZOU 4 , Rong-chang ZENG 1,5

- 1. Corrosion Laboratory for Light Metals, College of Materials Science and Engineering, Shandong University of Science and Technology, Qingdao 266590, China;
- 2. State Key Laboratory of Nonferrous Metals and Processes, GRINM Group Co., Ltd., Beijing 100088, China;
 - 3. School of Engineering, University of Newcastle, Callaghan, New South Wales, 2308, Australia;
 - 4. College of Chemical and Environmental Engineering, Shandong University of Science and Technology, Qingdao 266590, China;
 - 5. School of Materials Science and Engineering, Zhengzhou University, Zhengzhou 450002, China

Received 24 November 2022; accepted 10 August 2023

Abstract: The effect of oxalic acid (OA) etching on the formation mechanism and corrosion performance of in-situ steam Mg-Al layered double hydroxide (LDH) coatings on AM50 Mg alloy was investigated by exposing the intermetallic compounds (β -Mg₁₇Al₁₂ and AlMn) on the surface of the alloy. The results demonstrated that the presence of OA led to an increased fraction of intermetallic compounds on the Mg substrate. Mg-Al LDH nucleated and grew around the Al-Mn phase. The best corrosion resistance of LDH coating was obtained with the maximum thickness at a pickling time of 45 s, and the corrosion current density was reduced by three orders of magnitude compared to the substrate. Finally, the formation mechanism of Mg-Al LDH coating on AM50 Mg alloy was proposed.

Key words: magnesium alloy; oxalic acid; intermetallic compound; steam coating; layered double hydroxide; corrosion resistance

1 Introduction

As the lightest structural engineering material, magnesium (Mg) alloys have the advantages of low density, good casting performance, and mechanical properties, which have found applications in many fields including 3C electronic products, aerospace, and transportation [1,2]. However, the rapid corrosion rate of Mg is hampering its widespread applications. Hence, reducing the corrosion rate of Mg has become the driving force

for the continuous development of magnesium-based alloys [3–5].

Currently, the common methods to improve the corrosion resistance of Mg are as follows: elemental alloying, microstructure alteration, processing technology [6,7], and surface modification [8–11]. Unfortunately, alloying alone does not completely solve the corrosion problem, and thus surface modification process has become a practical strategy to improve the corrosion resistance of Mg and its alloys [12]. As a result, a large number of surface modification processes have been developed,

which include the chemical conversion treatments [13], layer by layer assembly [14], electrochemical deposition [15], micro-arc oxidation [16,17], and layered double hydroxides (LDHs) [18] and so on.

LDH coatings are a kind of layered bimetallic hydroxides, which have attracted much attention in recent years for their surface protection and functionalization properties [19,20]. LDHs can effectively capture aggressive ions and protect the substrates through anion exchange reactions in aggressive media [21]. The chemical formula of LDH is $[M_{1-x}^{2+}M_x^{3+}(OH)_2](A^{n-})_{x/n} \cdot mH_2O$, where M^{2+} and M^{3+} ions are bivalent and trivalent metallic cations, respectively, and A^{n-} represents an intercalated anion. Due to their unique sandwich structure, LDHs have been identified as a new type of intelligent coatings that can be used as nanocontainers by adjusting the type of interlayer anions [22,23].

A novel in-situ steam method for preparing LDH coating has been developed recently [24]. This method is simple, environmentally friendly, and inexpensive. The reactant used in this method is only ultrapure water, which is utilized as a steam source to facilitate the reaction. Due to the in-situ growth of LDH, the formed film binds closely to the surface of Mg and has excellent adhesion to the substrate. In the coating process, the sample is suspended 2–3 cm above the water level [24,25]. The required Al element for the reaction is basically from the dissolution of the Mg-Al alloy substrates and their intermetallic compounds. However, the Al3+ ions on the surface of the substrates that participate in the LDH formation reaction are insufficient for the growth of Mg-Al LDH coating. The obtained coating contains a large proportion of Mg(OH)₂ layer, which is soluble in chlorinecontaining environment and does not protect the substrates for a long time [26,27].

The Al element in the as-cast AM50 Mg alloy is present in the form of β -Mg₁₇Al₁₂ and AlMn phases, in addition to being partially solid-soluble in the Mg matrix [28]. Although the second phase particles provide the Al³⁺ ions needed for LDH growth in steam coating, they could also inhibit LDH formation to a certain extent [29].

However, the impact of the alloying elements and intermetallic compounds or second phase on the formation of LDH coatings has not been widely studied, particularly on in-situ steam LDH coating on Mg alloys. ISHIZAKI et al [30] prepared composite LDH films by steam coating treatment on Mg-Al alloys (AZ31, AZ61, and AZ91D). The coatings were composed of Mg(OH)2, AlOOH, and Mg-Al LDH for both AZ61 and AZ91D alloys. However, there is no AlOOH for the coating on AZ31 alloy. The fraction of AlOOH increases with increasing Al content in the alloys. It was noted that the content of Mg-Al LDH in the film on AZ61 alloy is the highest as compared to that on AZ31 and AZ91D alloys. The corrosion resistance of the coatings depends on the thickness and LDH content of the coating. It is evident that the presence of Al as an alloying element is beneficial to the formation of Mg-Al LDH coating for improved corrosion resistance. On the contrary, a high Al content inhibits the formation of LDH coating on AZ91 Mg alloy. The content of Al in the matrix and intermetallic compounds for effective formation of LDH coating on Mg-Al alloys has not been known

CHEN et al [31] have reviewed a large number corrosion protection conversion coatings available for Mg alloys, and it was noted that the best coatings involve pretreatment. Acid etching has been used as a pretreatment process for vapor deposition coatings on Mg alloys [32–34]. Pickling treatment also improved the surface energy and increased roughness of the substrate and thus increased the adhesion of the coating [35,36]. In our previous work [37], it was found that area fraction of the second phases in extruded AZ80 Mg alloys increased after citric acid (CA) etching, which resulted in a denser and thicker LDH formation. The observation of C=O and C-O groups in the XPS spectra suggested that CA has a strong complexing ability with metallic ions, which promotes the formation of Mg-Al LDH coating. Oxalic acid (OA) has a strong coordination effect [38,39]. OA can form oxalate complexes with Mg²⁺ and Al³⁺ [40], which can improve the distribution of nucleation sites of LDH coatings on the alloy surface. It is worth mentioning that the microstructure of as-extruded Mg alloy is generally uniform and homogeneous. In contrast, the composition of the microstructure in the as-cast Mg alloys is heterogeneous.

This study aims to investigate the effect of OA etching on the exposure of surface intermetallic compounds (Al-containing species) and the

formation mechanism and corrosion resistance of in-situ steam Mg-Al LDH coatings on as-cast AM50 Mg alloy. Further, the influence of the distribution of the intermetallic compounds on the nucleation and growth of the in-situ steam LDH coating was studied.

2 Experimental

2.1 Materials

An as-cast AM50 Mg alloy (composition: 4.4–4.5 wt.% Al, 0.22 wt.% Zn, 0.2–0.6 wt.% Mn, 0.01 wt.% Si, 0.01 wt.% Cu, 0.002 wt.% Ni, 0.004 wt.% Fe, and the rest is Mg) with dimensions of 20 mm × 20 mm × 5 mm (supplied by Shandong Yinguang Yuyuan Light Metal Precise Forming Co., Ltd., China) was used as the substrate in this study. The alloy samples were sanded to 2500[#] with silicon carbide paper prior to the experiments and then rinsed with deionized water and air dried.

2.2 Preparation of steam coating

A procedure of the LDH coating by in-situ steam method was illustrated in Fig. 1. The as-cast AM50 Mg alloys were etched with 10 g/L OA solution for 15, 30, 45, and 60 s, respectively, and then cleaned with deionized water and absolute ethanol. A 20 mL ultrapure water was added to a 100 mL PTFE container. The OA-pretreated sample was suspended 2 cm above the water level using a cotton thread. The setup was enclosed in an autoclave and transferred to an oven and heated to 433 K for 6 h to obtain the LDH coating. The samples were named OA/AM50-15s, OA/AM50-30s, OA/AM50-45s, and OA/AM50-60s based on the etching time, and the coated samples after the insitu steam reaction are designated as OA/LDH-15s, OA/LDH-30s, OA/LDH-45s, and OA/LDH-60s, respectively.

2.3 Coating characterization

2.3.1 Surface morphology and composition analysis

An optical microscope (OM, Olympus-GX41, Japan) was used to capture the microstructure of the samples and analytical software (ImageJ) was used to calculate the surface fraction of the second phases. A three-dimensional (3D) topography and the surface roughness of the samples before and after OA etching were measured using a 3D topography instrument (Zeta-20, Bruker Contour GT-K optical profiler). The average roughness (R_a) of the samples was calculated based on three measurements. The compositions of the LDH coatings and the substrates were determined by an X-ray diffractometer (XRD, Rigaku Ultima IV, Japan) with Cu K_{α} target (λ =0.154 nm). The parameters used were: scanning angle range of 5°-80° and scanning speed of 8 (°)/min. The chemical bonds and functional groups in different kinds of LDH coatings were analyzed by a Fourier transform infrared spectrometer (FT-IR, Thermo Fisher Scientific, Nicolet 380, USA) with a wavenumber range of 4000-400 cm⁻¹ and a resolution of 1 cm⁻¹ at room temperature. The elemental presence, valence state, and functional group of LDH coating were analyzed by X-ray photoelectron spectroscopy (XPS, ESCALAB XI+, Thermo Fisher Scientific, USA). An Al target was used with an energy resolution of 100 eV broad spectrum and 20 eV narrow spectrum and the charge correction was carried out with C element (284.6 eV).

2.3.2 Corrosion performance assessment

The corrosion performance was evaluated using an electrochemical step-up and a potentiostat (PARSTAT 2273, Princeton Instruments Co., USA). The electrochemical step-up consisted of a conventional three-electrode cell, i.e. working electrode (sample to be tested), reference electrode

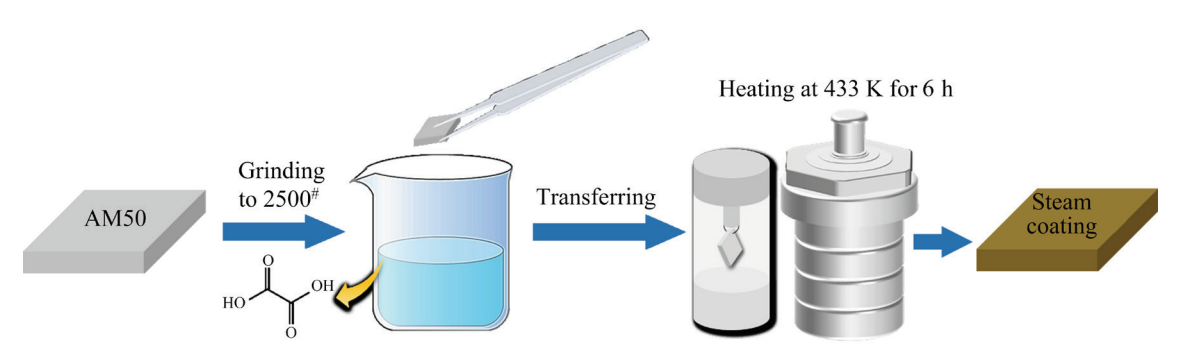


Fig. 1 Schematic diagram of experimental process for preparing steam coating on AM50 Mg alloy

(saturated KCl-glycury electrode) and counter electrode (platinum electrode). All tests were carried out in 3.5 wt.% NaCl solution at room temperature. The scan rate of the potentiodynamic polarization curve was 2 mV/s. According to Eq. (1), the corrosion current density J_{corr} is converted into a corrosion rate v, where A is the relative atomic mass, n is the number of electrons gained or lost, and ρ is the density of the metal material.

$$v = \frac{3.27 \, AJ_{\text{corr}}}{n\rho} \tag{1}$$

Electrochemical impedance spectroscopy (EIS) analysis was performed in the frequency range from 10 mHz to 100 kHz with 10 mV amplitude. Equivalent circuit modeling of the obtained EIS spectra was done using software (ZSimpWin). To

further analyze the corrosion resistance of the coating, a salt spray experiment was carried out using 5 wt.% NaCl solution. Photographs were taken at different periods.

3 Results

3.1 Surface topography after OA etching

Figure 2 shows the microstructure and area fraction of intermetallic compounds on as-cast AM50 Mg alloy surface after OA etching. As seen in Fig. 2(a), there are a few second phase particles on the surface of polished as-cast AM50 Mg alloy. In Figs. 2(b-d), the exposed second phase on the alloy surface increases with the increase of acid etching time, and the number of the exposed second phase particles is the largest when the OA etching

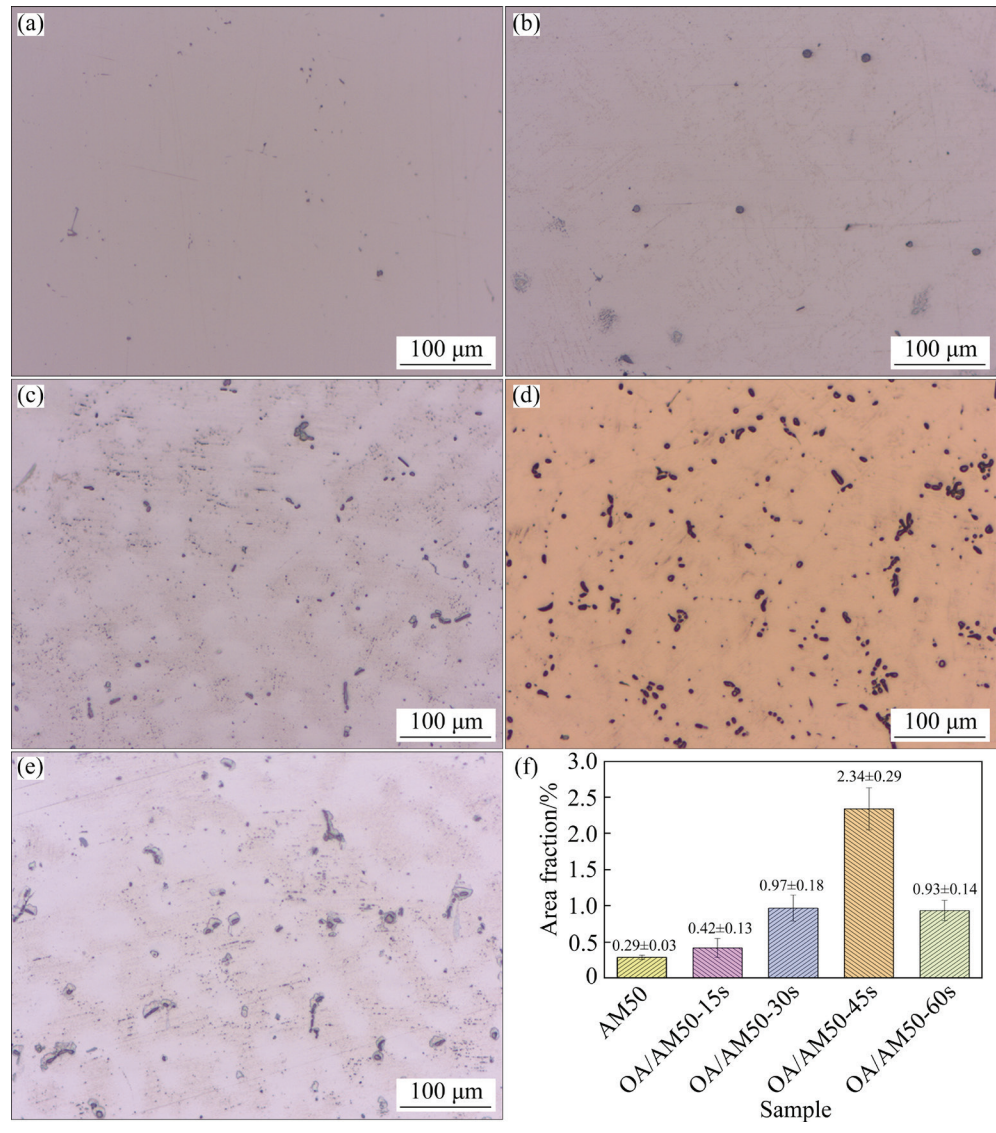


Fig. 2 Metallographic microstructures of polished AM50 Mg alloy (a), OA/AM50-15s (b), OA/AM50-30s (c), OA/AM50-45s (d), OA/AM50-60s (e) and corresponding area fraction of second phase (f)

time is 45 s. With further increase in time, the number of second phase particles on the surface of OA/AM50-60s Mg alloy decreases, which is due to extensive corrosion (Fig. 2(e)). The area fraction of the Al-rich phase particles was calculated using the software ImageJ, and the histogram of the particles is presented in Fig. 2(f). The acid etching significantly increased the area fraction of the second phase, and the area fraction of the Al-rich phase particles on the surface of OA/AM50-45s sample reached the maximum. It was noted that when the etching time in the OA solution was long (60 s), the Al-rich phase on the surface of the alloy was damaged to some extent and the exposed second phase particles were reduced. Therefore, when the acid etching time is appropriate, the second phase particles on the surface will be fully exposed, and the nucleation sites can be increased, which is helpful for the subsequent growth of LDH coating.

Figure 3 shows the XRD patterns of the as-cast AM50 magnesium alloy after different OA etching time. Strong diffraction peaks of AlMn and Al₈Mn₅ were found in all specimens. Those diffraction peaks tend to increase with the increase of OA etching time, which is consistent with the metallographic micrographs in Fig. 2. Moreover, the OA/AM50-45s sample has the strongest diffraction peaks for the AlMn and Al₈Mn₅ phases, which indicates that the most Al-rich phases can be exposed under this condition. Therefore, it is favorable for the subsequent LDH growth.

The microstructures of AM50 after polishing and etching with OA are shown in Figs. 4(a-e). It

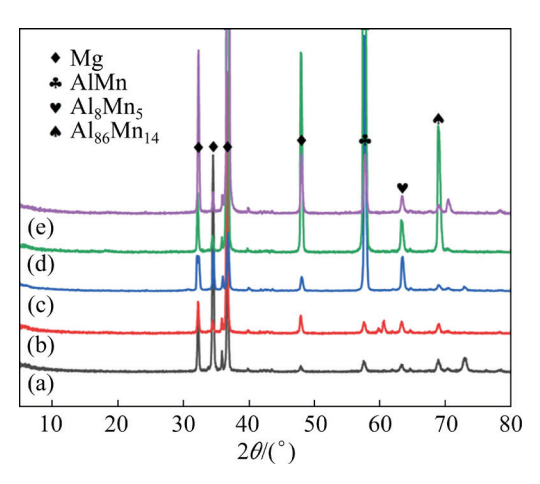


Fig. 3 XRD patterns of as-cast AM50 Mg alloy (a), OA/AM50-15s (b), OA/AM50-30s (c), OA/AM50-45s (d) and OA/AM50-60s (e)

can be seen that the Al-rich eutectic films of AM50 are mainly granular and flaky, and Al-rich phase particles on the surface of the alloy are exposed significantly after OA etching. There are few Al-rich phase particles exposed on the polished AM50 surface, as seen in Fig. 4(a). It is worth noting that, in Figs. 4(b-d), with the increase of OA etching time, the number of Al-rich phase particles on the surface of AM50 increases, and the area fraction of the second phase particles reaches the maximum after 45 s treatment. It is found that the area fraction of the Al-rich phase does not continue to increase with a further increase in the etching time. Instead, there are pits on the alloy surface. This can be due to the long time acid treatment,

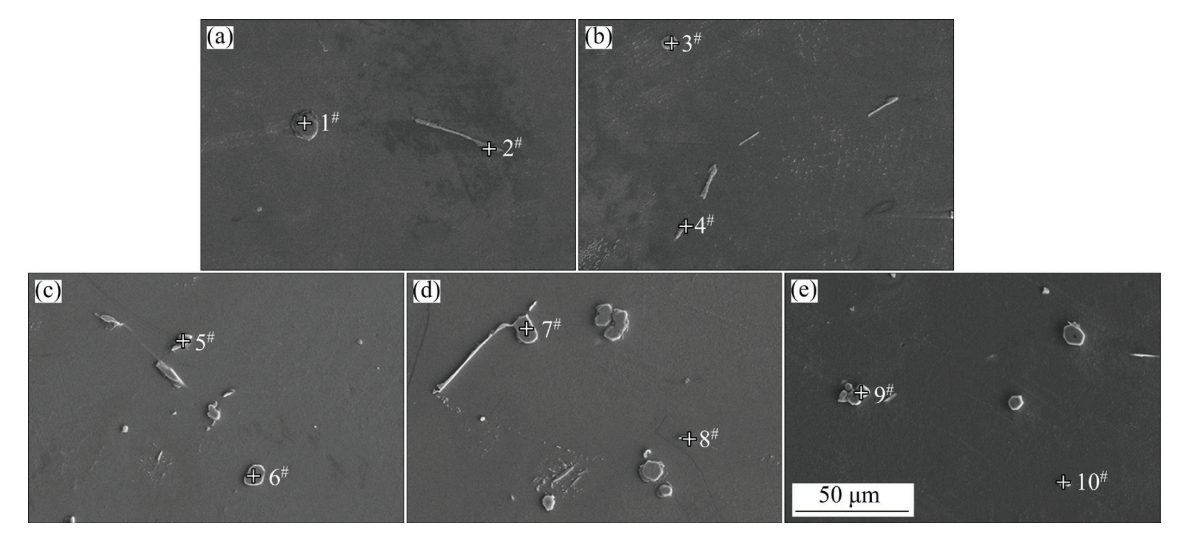


Fig. 4 SEM images of polished AM50 Mg alloy (a), OA/AM50-15s (b), OA/AM50-30s (c), OA/AM50-45s (d) and OA/AM50-60s (e)

resulting in corrosion pits and shedding of the second phase particles. The elemental composition of the AM50 surface after OA treatment (Fig. 4) is shown in Table 1. The elemental composition shows a large amount of C and O present on the surface, which can be attributed to the oxalate produced by the complexation of the dibasic strong acid (oxalic acid) with the matrix. It can be observed from the element composition (Points 1[#]–10[#]) that the Al/Mn molar ratios of the granular phase are close to 4:1 and 1:1, respectively. The result suggests that the second phase is Al₄Mn phase as well as AlMn phase. The morphology of the flakes with Mg/Al molar ratio close to 17:12 is designated as the Mg₁₇Al₁₂ phase. Therefore, the main second phase particles in AM50 are AlMn, Al₄Mn, and β -Mg₁₇Al₁₂. At the same time, appropriate etching time may not cause damage to the flake β -Mg₁₇Al₁₂ phase and granular AlMn phase, which is conducive to the growth of subsequent LDH coating.

Figure 5 shows the 3D morphology and surface roughness (R_a) of each sample after OA etching. The R_a is arranged in ascending order: AM50 after polishing ((0.075±0.013) µm) < OA/AM50-15s ((0.089±0.018) µm) < OA/AM50-30s ((0.098±0.015) µm) < OA/AM50-60s ((0.108±0.017) µm) < OA/AM50-45s ((0.125±0.02) µm). The R_a increases with increase of the etching time. It is noted that when the etching time reaches 60 s, the R_a decreases, which may be due to excessive corrosion. As the α -Mg matrix dissolves, the β -Mg₁₇Al₁₂ phase and AlMn phase on the surface of the alloy increase, and the roughness increases.

Table 1 Elemental compositions of selected points on surface of AM50 Mg alloy in Fig. 4 (at.%)

Point	C	O	Mg	Al	Mn
1#	35.00	20.15	38.42	4.61	1.82
2#	26.18	3.72	66.27	3.39	0.43
3#	29.05	6.13	5.27	47.64	11.91
4#	35.24	3.82	36.58	24.36	_
5#	35.08	20.67	5.03	20.05	19.16
$6^{\#}$	32.69	16.41	9.60	33.04	8.26
7#	44.06	6.86	3.14	23.65	22.28
8#	37.17	4.36	34.28	24.19	_
9#	38.41	18.70	5.08	19.37	18.45
10#	8.83	3.34	51.29	36.54	-

3.2 Surface coating characteristics

Figure 6(a) shows the XRD patterns of AM50 and the LDH coatings after different OA treatment time. The diffraction peaks of LDH appear at both 11.3° and 22.6°, corresponding to (003) and (006) crystal planes of carbonate intercalated LDH, respectively. This indicates that the LDH coating is successfully prepared on the substrate. The LDH diffraction peaks of the samples etched with OA for 45 s are the strongest, which suggests that the LDH content of the coating generated under this condition is the highest. The characteristic diffraction peaks of brucite-type Mg(OH)₂ appear at 2θ =18.4°, 37.8°, 58.6° and 62°. Thus, the LDH coatings prepared in this study are composed of Mg-Al-CO₃² LDH and Mg(OH)₂, which is consistent with the literature [24,30].

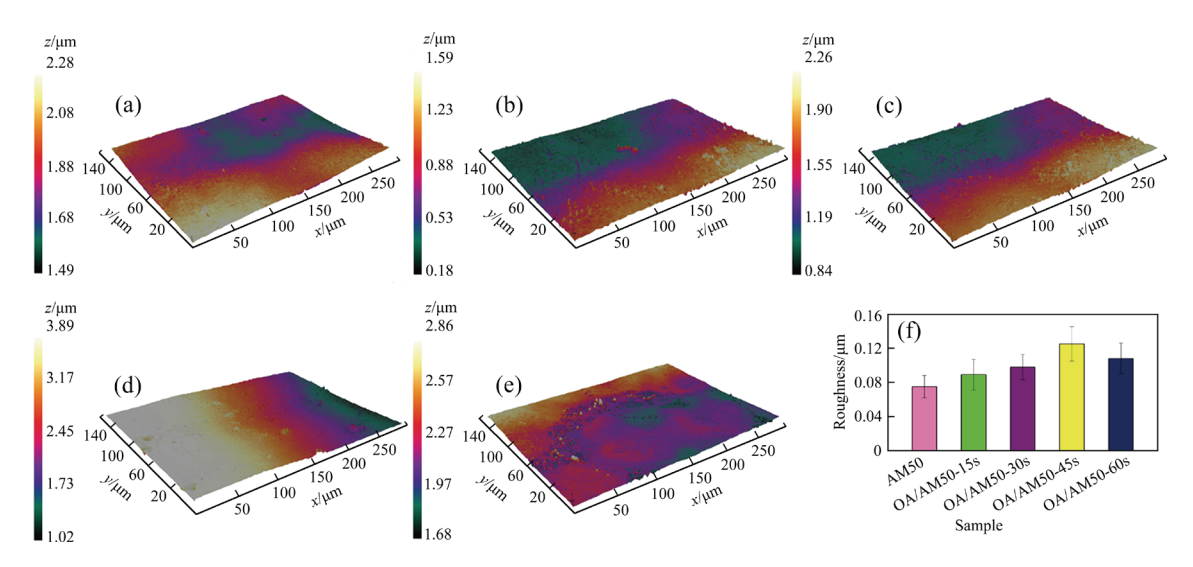


Fig. 5 3D surface morphologies of polished AM50 Mg alloy (a), OA/AM50-15s (b), OA/AM50-30s (c), OA/AM50-45s (d), OA/AM50-60s (e) and corresponding roughness (f)

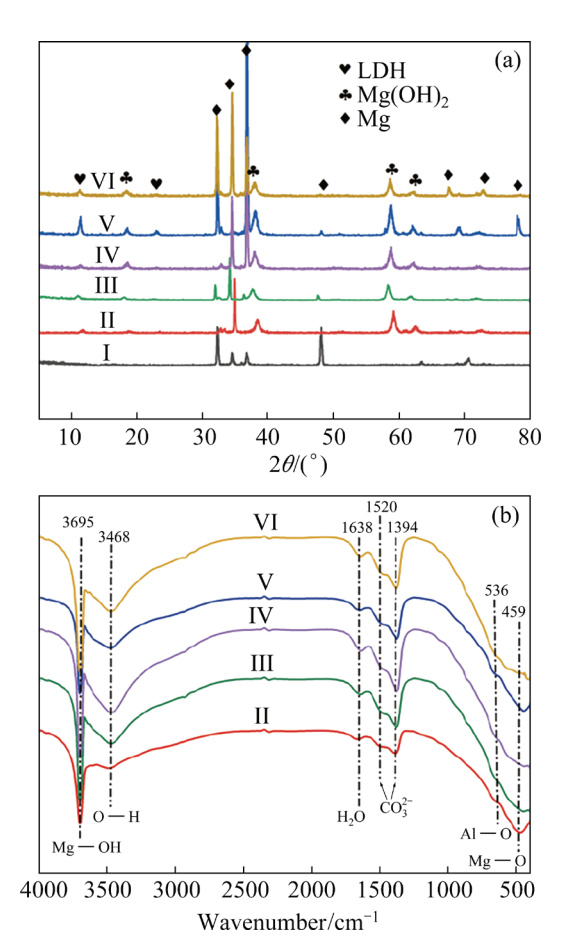


Fig. 6 XRD patterns (a) and FT-IR spectra (b) of AM50 Mg (I), LDH (II), OA/LDH-15s (III), OA/LDH-30s (IV), OA/LDH-45s (V) and OA/LDH-60s (VI)

Figure 6(b) shows the FT-IR spectra of AM50 and the LDH coatings after OA treatment. It can be seen that the positions and numbers of the absorption peaks of each functional group under different conditions are the same, while the intensity of the absorption peaks is different. There is an absorption peak of Mg—OH at 3695 cm⁻¹ and an absorption peak of O—H at 3468 cm⁻¹, which are caused by the reaction of water vapor with AM50, thus forming product of Mg(OH)₂. The absorption peak at 1638 cm⁻¹ corresponds to —OH in water molecules, and 1520 and 1394 cm⁻¹ are the absorption peaks of intercalation ion CO_3^{2-} , indicating that the intercalation anion between LDH laminates is CO_3^{2-} , which is in line with the XRD results (Fig. 6(a)). The stretching vibration of Al — O at a wavenumber of 536 cm⁻¹ and the stretching vibration of Mg-O at 459 cm⁻¹ are attributed to the main laminate structure of LDH. The results suggest that the LDH coating is successfully prepared on the surface of the substrate

by the steam method, and the coatings are composed of Mg(OH)₂ and Mg-Al-CO₃²⁻ LDH.

Figure 7 shows the SEM images of the LDH coatings after different OA treatment time. It can be seen that the LDH coating without OA etching in Fig. 7(a) is loose, and the size of the nano-sheets is smaller and different from each other. As can be seen from Figs. 7(b-e), the compactness of the obtained coatings is effectively improved after OA etching and the growth of LDH nano-sheets becomes much more uniform compared to the sample without OA etching. Among the samples, OA/LDH-45s sample possesses the densest morphology, and the needle-like nano-sheets grow vertically, which almost completely cover the surface of the alloy substrate. When the etching time is up to 60 s, the gap between the nano-sheets begins to increase and the morphology is not as uniform as that of the OA/LDH-45s sample, which is consistent with the results of the metallographic test. Although the increase of the β -Mg₁₇Al₁₂ phase increases the corrosion resistance of the alloy, excessive acid etching causes damage to the alloy surface, making the second phase particles dissolve or fall off, resulting in the loss of Al³⁺ ions. Figure 7(f) shows the EDS data (average of 3 points) corresponding to Figs. 7(a-e). The data show that the coating is mainly composed of C, O, Mg and Al, and the most abundant elements in the coating are O and Mg, indicating that the coating is mainly composed of Mg(OH)₂. The increased contents of C and Al indicate that the content of Mg-Al-CO₃² LDH increases after OA etching. The content of Al in the sample of OA/AM50-45s reaches 3.36, which is twice as much as that in the LDH coating without acid etching, demonstrating that the activation of OA increases the content of LDH in the coating. It is noted that the Al content in the OA/AM50-60s samples decreases, which is consistent with the result of the SEM image analysis.

Figure 8 shows the longitudinal cross-sectional views and element distribution of different LDH coatings on AM50. The thickness of LDH coating prepared by OA etching combined with the in-situ steam method on the surface of AM50 is larger, with the maximum thickness of 61.05 μ m (OA/LDH-45s). This coating thickness is nearly twice the thickness of LDH coating without OA etching (32.78 μ m). As shown in Figs. 8(a–d), with the increase of etching time (from 15 to 45 s), the

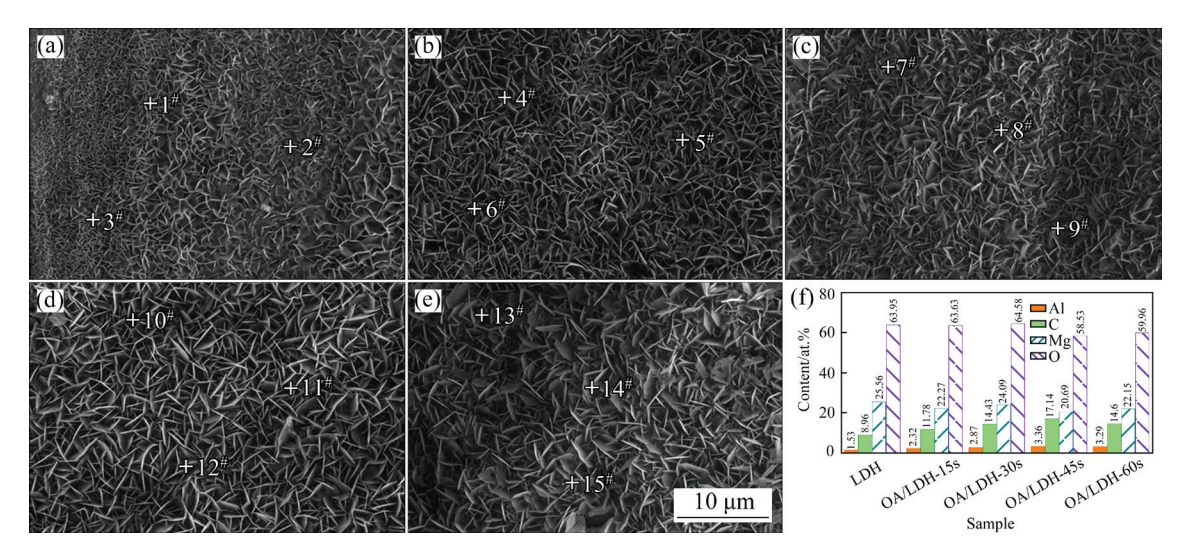


Fig. 7 SEM images of LDH (a), OA/LDH-15s (b), OA/LDH-30s (c), OA/LDH-45s (d), OA/LDH-60s (e) and corresponding EDS data (f)

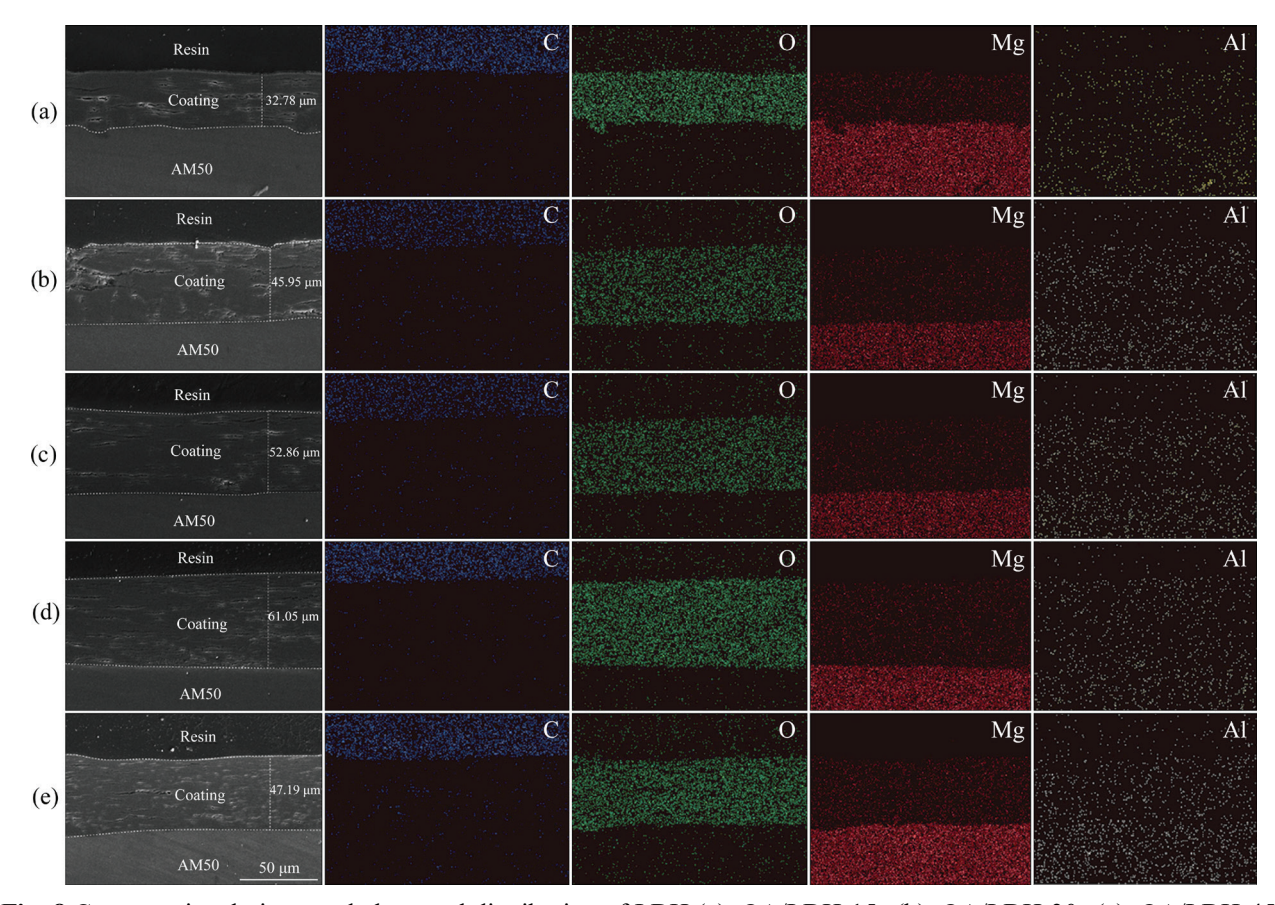


Fig. 8 Cross-sectional views and elemental distribution of LDH (a), OA/LDH-15s (b), OA/LDH-30s (c), OA/LDH-45s (d) and OA/LDH-60s (e)

thickness of LDH coating increases, and the microcracks in the coating decrease gradually. After activation by OA, more second phase particles are exposed on the surface of the substrate, and the amount of LDH generated increases, thus the

thickness and compactness of the coating are significantly improved. It is worth mentioning that the LDH coating prepared by in-situ steam method has grown from inside to outside as the Mg and Al sources are from the Mg alloy substrate, and hence there are fine cracks inside the film. It is observed that when the OA etching time reaches 60 s, the thickness of the coating decreases, which is consistent with the results of metallographic test and 3D morphology test. Although acid etching can make use of micro galvanic corrosion between the α -Mg phase and the second phase particles, changing the distribution of the second phase particles, excessive etching will cause damage to the Al-rich phase, which is easy to cause overcorrosion and dissolution or shedding of the second phase particles.

3.3 Corrosion resistance

The polarization curves of AM50, LDH, OA/LDH-15s, OA/LDH-30s, OA/LDH-45s and OA/LDH-60s samples in 3.5 wt.% NaCl solution are shown in Fig. 9. Due to the unusual behavior of the Mg alloy during anodic dissolution, the anodic region of the polarization curve shows very pronounced passivation and the traditional Tafel extrapolation method of calculating the corrosion current density (J_{corr}) is not accurate enough, so only the cathodic polarisation region was used to obtain the J_{corr} and the data obtained are listed in Table 2. The values of corrosion potential (φ_{corr}) reflect the thermodynamic properties of the coatings, i.e., the higher the φ_{corr} value, the more stable the coating; the J_{corr} values reflect the anti-corrosion performance of the coatings, i.e., the lower the J_{corr} , the better the corrosion resistance of the coating. Table 2 indicates that the φ_{corr} of LDH coating obtained by OA treatment is higher than

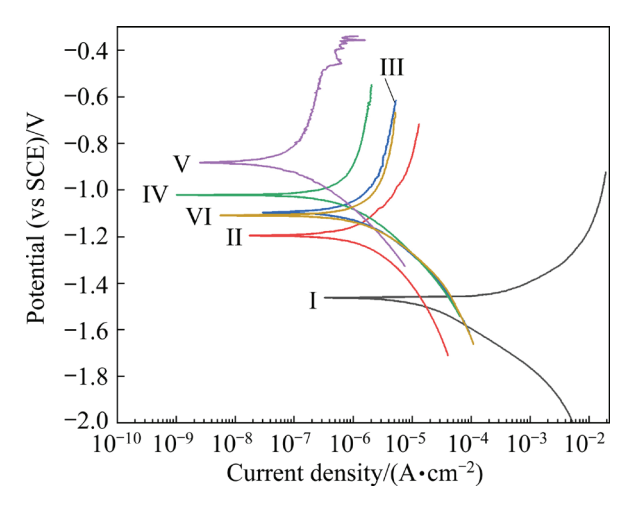


Fig. 9 Potentiodynamic polarization curves of as-cast AM50 (I), LDH (II), OA/LDH-15s (III), OA/LDH-30s (IV), OA/LDH-45s (V) and OA/LDH-60s (VI)

Table 2 Fitted data for polarization curves of samples in Fig. 9

Sample	$\varphi_{\mathrm{corr}}(\mathrm{vs}\;\mathrm{SCE})/V$	$J_{ m corr}/$ $({ m A\cdot cm}^{-2})$	ν/ (μm·a ⁻¹)
AM50	-1.46	2.25×10 ⁻⁵	4.58×10 ⁻⁴
LDH	-1.20	1.55×10^{-6}	3.16×10^{-5}
OA/LDH-15s	-1.10	1.64×10^{-6}	3.34×10^{-5}
OA/LDH-30s	-1.02	2.89×10^{-7}	5.89×10^{-6}
OA/LDH-45s	-0.88	6.49×10^{-8}	1.32×10^{-6}
OA/LDH-60s	-1.11	1.10×10^{-6}	2.24×10^{-5}

that of AM50, and the OA/LDH-45s sample has the largest φ_{corr} value, the smallest J_{corr} value as well as the smallest corrosion rate (v) value. The OA/LDH-45s sample shows repeated damage and repair phenomena in the anodic polarization region, suggesting that the corrosive Cl⁻ destroys the LDH coating and is in direct contact with the Mg alloy substrate. This shows that the steam LDH coating has strong ion exchange ability, and due to the anion exchange between the LDH layers, the corrosion products can protect the substrate.

Figure 10 illustrates the EIS curves of AM50 and LDH coatings obtained under different etching conditions in 3.5 wt.% NaCl solution. In the low frequency region of Fig. 10(a), impedance modulus value |Z| reflects the corrosion resistance of the sample. The impedance modulus |Z| of each sample is in the ascending order: AM50 < OA/LDH-60s < LDH < OA/LDH-15s < OA/LDH-30s < OA/LDH-45s. Therefore, the sample pretreated with OA for 45 s has the best corrosion resistance. In Figs. 10(b-d), show capacitive curves two corresponding to the internal dense layer and external loose layer of the LDH coating, which is consistent with our previously published work [37]. The larger the curvature radius of the impedance arc in the low frequency region, the better the corrosion resistance of the sample. As can be seen in Fig. 10(b), the curvature radius of the OA/LDH-45s sample is the greatest in the low frequency region, and the sloping line at low frequencies shows the characteristics of the diffusion process of the ionic material at the interface. The radius of the impedance curve in the low frequency region is much larger for the OA/LDH-45s sample than that for the rest of the samples, indicating that the OA/LDH-45s sample has the highest electrochemical capacitance and the best corrosion resistance,

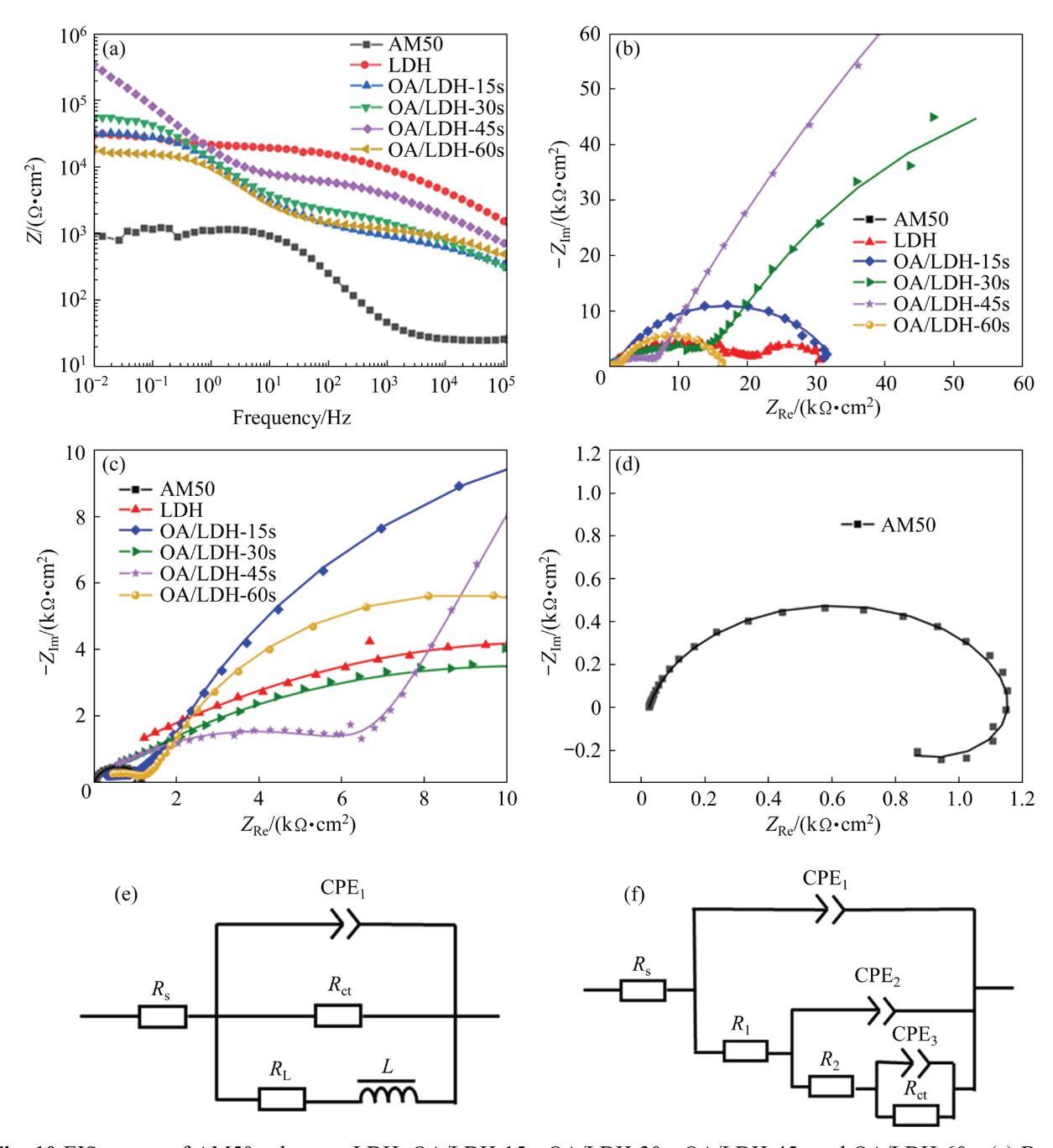


Fig. 10 EIS curves of AM50 substrate, LDH, OA/LDH-15s, OA/LDH-30s, OA/LDH-45s and OA/LDH-60s: (a) Bode plots; (b) Nyquist plots; (c) Enlarged Nyquist plots; (d) Enlarged Nyquist plot of AM50 substrate; (e, f) EC diagrams of AM50 substrate and LDH coating, respectively

which can be attributed to the higher coating thickness and its increased LDH content after OA etching. It is worth noting that the curvature radius of OA/LDH-60s sample becomes smaller, indicating that the long-term OA etching damages the surface of AM50 and can no longer promote the growth of the in-situ LDH coating.

Figures 10(e, f) show the equivalent circuit (EC) diagrams of AM50 and LDH coating, respectively, and Table 3 shows the fitting results.

The EC diagram for AM50 substrate (Fig. 10(e)) is composed of constant phase element CPE₁ and charge transfer resistance ($R_{\rm ct}$) in the high frequency region, indicating the formation of a loose film of corrosion products on AM50. The $R_{\rm L}$ and L in the low frequency region indicate the presence of corrosion pits on the substrate and the shedding of the corrosion film. Figure 10(f) shows the EC diagram of LDH coatings obtained under different etching conditions, in which $R_{\rm s}$ is solution resistance,

Table 3 Electrochemical data from EIS fits data in Fig. 10

Parameter				Sample		
Parameter	AM50	LDH	OA/LDH-15s	OA/LDH-30s	OA/LDH-45s	OA/LDH-60s
$R_{\rm s}/(\Omega\cdot{\rm cm}^2)$	24.87	110.25	45.38	40.38	39.52	70.69
$CPE_1/(\Omega^{-1}\cdot cm^{-2}\cdot s^n)$	1.44×10^{-5}	1.05×10^{-9}	3.36×10^{-6}	5.95×10^{-6}	5.58×10^{-8}	2.63×10^{-6}
n_1	0.8	0.95	0.49	0.47	0.73	0.48
$R_1/(\Omega \cdot \text{cm}^2)$	_	9.10×10^{2}	1.06×10^{2}	2.73×10^{3}	1.91×10^{3}	1.38×10^{3}
$CPE_2/(\Omega^{-1}\cdot cm^{-2}\cdot s^n)$	_	1.28×10 ⁻⁶	6.55×10^{-6}	8.13×10^{-6}	2.90×10^{-7}	8.81×10^{-6}
n_2	_	0.46	0.79	0.86	0.48	0.85
$R_2/(\Omega \cdot \mathrm{cm}^2)$	_	2.12×10^{4}	2.11×10^{3}	8.21×10^{3}	6.55×10^{3}	1.82×10^{3}
$CPE_3/(\Omega^{-1}\cdot cm^{-2}\cdot s^n)$	_	1.46×10^{-4}	7.59×10^{-6}	6.28×10^{-6}	1.39×10^{-5}	7.33×10^{-6}
n_3	_	0.84	0.84	0.87	0.78	0.85
$R_{\rm ct}/(\Omega\cdot{\rm cm}^2)$	6.61×10^{2}	9.48×10^{3}	3.02×10^{4}	5.05×10^4	5.42×10^{5}	1.35×10^{4}
$R_{\rm L}/(\Omega\cdot{\rm cm}^2)$	5.13×10^{2}	_	_	_	-	_
$L/(\mathrm{H}\cdot\mathrm{cm}^{-2})$	2.14×10^{2}	_	_	_	_	_

n, n_1 , n_2 and n_3 are exponents of constant phase angle elements

 R_1 and R_2 are the loose outer resistance and the dense inner resistance of the steam LDH coating, respectively. The higher the value of $R_{\rm ct}$ is, the better the corrosion resistance of the sample is. The $R_{\rm ct}$ value is the highest for the sample pretreated with OA for 45 s, hence the LDH coating obtained under this condition has the best effect.

Figure 11 shows the photographs of AM50 and LDH coatings obtained under different treatment conditions, exposed to a neutral salt spray condition of 5 wt.% NaCl solution for different periods. When the test period was 72 h, the AM50 substrate (Fig. 11(a₂)) was severely corroded, whereas for the LDH coated substrate, the coating (Figs. $11(b_2-f_2)$) remained intact, but the surface color was darkened. As can be seen in Figs. 11(a₃) and (b₃), corrosion pits appeared on the surface of AM50 substrate and the LDH coating without OA etching after 144 h (highlighted with the black ellipse). As observed in Figs. 11(c₃-f₃), a large number of white corrosion products appeared on the surface of LDH coating with the continuous erosion effect of Cl⁻ ions, but the coating remained intact. After 360 h test, the corrosion pits spread continuously, and the corrosion was aggravated by the diffusion of Cl⁻ in the microcracks and holes of the coating. When the exposure time was extended to 600 h, the number of corrosion pits in the OA/LDH-45s sample (Fig. 11(e₅)) was minimal and the integrity of the coating was the best, whereas AM50 exhibited serious damage, indicating that the LDH prepared under this condition can protect the substrate.

To further evaluate the degree of corrosion, analyze the morphology and elements of corrosion products, and verify the protection mechanism, the microscopic morphology of each sample after 600 h salt spray experiment was characterized by SEM. As shown in Fig. 12(a), the AM50 substrate was severely corroded under the salt spray condition of 600 h, resulting in many cracks and accumulation of corrosion products on the surface. The surface of the LDH coating without OA etching, as shown in Fig. 12(b), also had microcracks, and the corrosion was severe in some areas. As can be seen in Figs. 12(c-e), the integrity of the LDH coating after the salt spray test continued to improve with the prolongation of the OA etching time. There were no cracks or corrosion pits on the surface, but only a small amount of corrosion product was accumulated and the morphology of LDH nano-sheets was visible. In particular, the OA/LDH-45s sample retained the most complete morphology, indicating that it can still provide long-term protection for Mg alloy in the corrosion environment with high Cl⁻ content. From the elemental composition of the sample after corrosion, as shown in Table 4, it is clear that corrosion product is rich in Mg and O, and hence it can be concluded that the main corrosion product is Mg(OH)2. Notably, the OA/LDH-45s samples had the highest LDH content

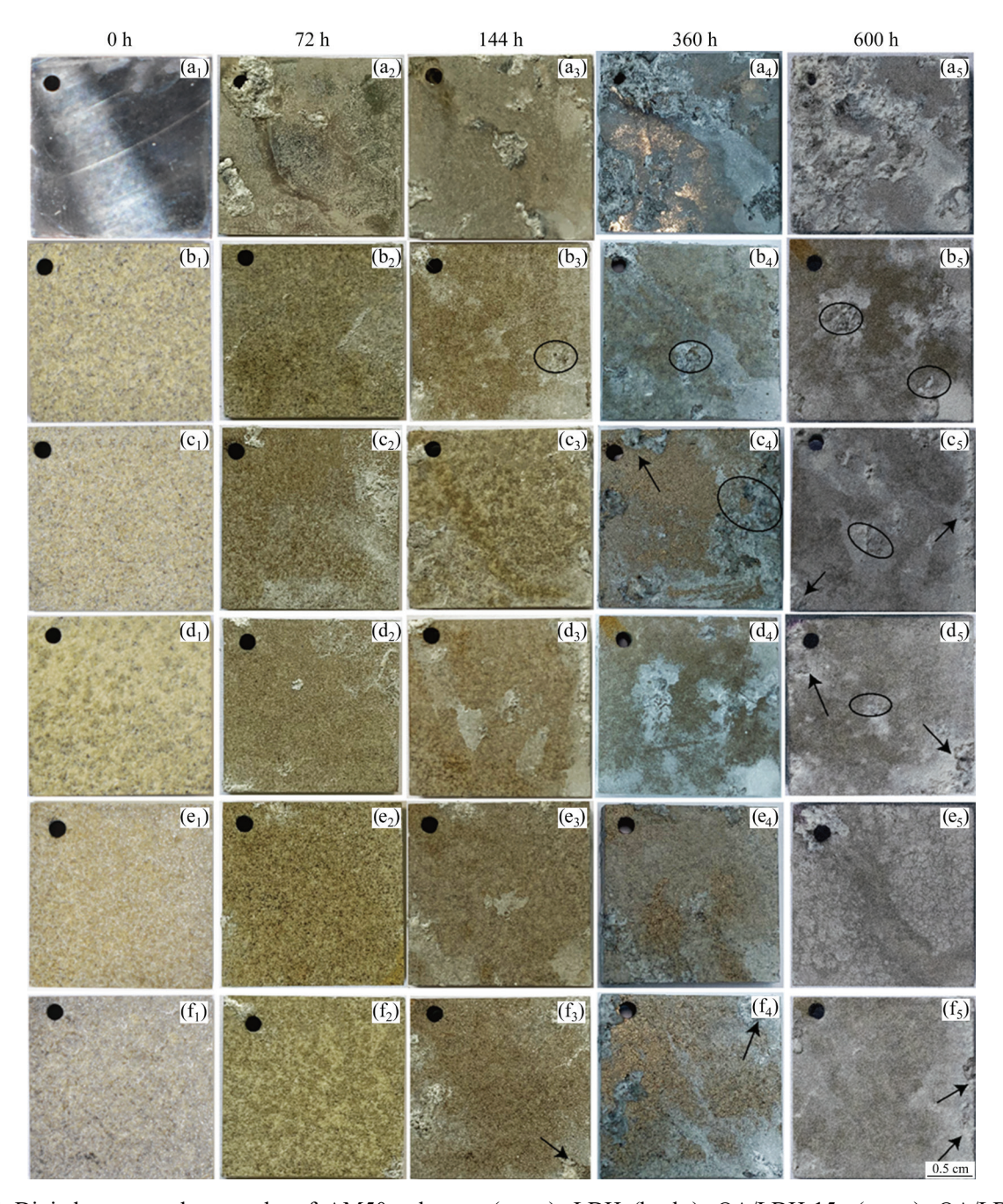


Fig. 11 Digital camera photographs of AM50 substrate (a_1-a_5) , LDH (b_1-b_5) , OA/LDH-15s (c_1-c_5) , OA/LDH-30s (d_1-d_5) , OA/LDH-45s (e_1-e_5) and OA/LDH-60s (f_1-f_5) under neutral salt spray conditions of 5 wt.% NaCl solution for different periods

prior to corrosion, and after 600 h of salt spray, the OA/LDH-45s samples also had the highest C and Al contents, indicating that the samples still had the highest LDH content. This may be due to the excellent ion exchange of LDH, which allows the conversion of Mg-Al-CO₃²⁻ LDH to Mg-Al-Cl-LDH over a longer immersion time, with LDH structure retained. Based on the SEM results, it can be concluded that the higher the LDH content, the better the corrosion resistance of the coating.

3.4 Formation mechanism of LDH coating

3.4.1 Influence of second phase on growth of LDH coating

To further analyze the influence of the second phase particles on the growth of the LDH coating on AM50 (the optimized etching time was fixed at 45 s), samples were grown for 0.5, 1.5 and 3 h, respectively. Figure 13 shows the XRD patterns of the samples with reaction time of 0.5, 1.5, and 3 h. It can be seen that the diffraction peaks of Mg(OH)₂

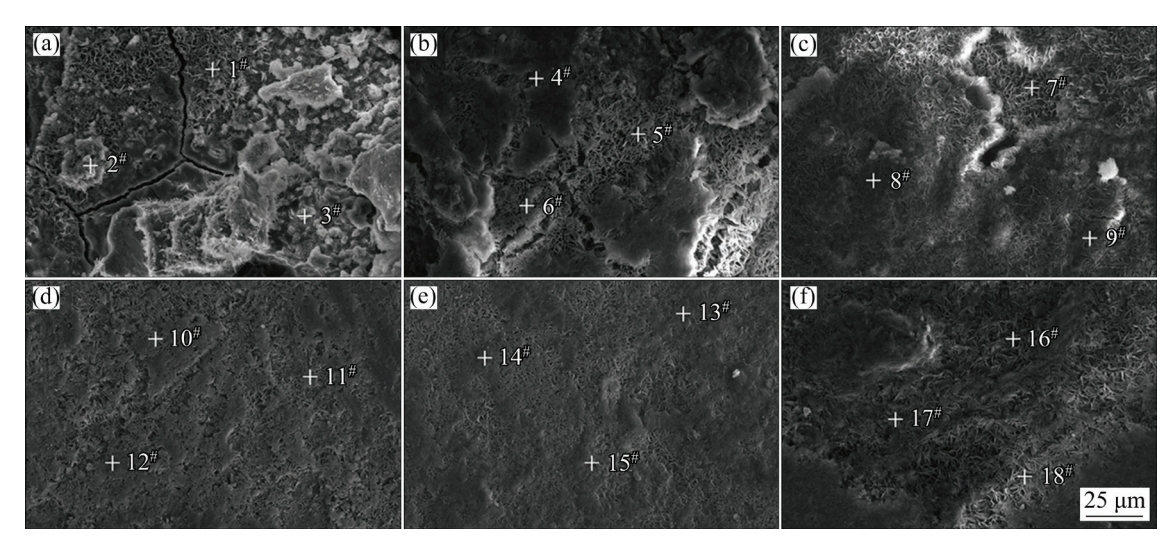


Fig. 12 SEM micrographs of AM50 (a), LDH (b), OA/LDH-15s (c), OA/LDH-30s (d), OA/LDH-45s (e) and OA/LDH-60s (f) under neutral salt spray conditions in 5 wt.% NaCl solution for 600 h

Table 4 Elemental compositions on LDH coatings shown in Fig. 12 (at.%)

Sample	С	О	Mg	Al	Na
AM50	16.57±1.20	60.47 ± 4.35	19.33±0.89	_	3.63±0.13
LDH	13.37 ± 2.06	60.16 ± 3.57	23.36±1.45	0.18 ± 0.06	2.92 ± 0.58
OA/LDH-15s	11.36 ± 1.62	64.42 ± 2.68	21.87 ± 0.76	0.50 ± 0.11	1.86 ± 0.19
OA/LDH-30s	13.95±2.46	63.22 ± 4.88	21.20±2.93	0.81 ± 0.19	0.82 ± 0.06
OA/LDH-45s	14.59±1.35	63.92 ± 4.67	18.97±1.38	1.12±0.25	1.41 ± 0.53
OA/LDH-60s	15.55±1.56	64.40 ± 5.34	18.22 ± 2.01	0.67 ± 0.22	1.16 ± 0.31

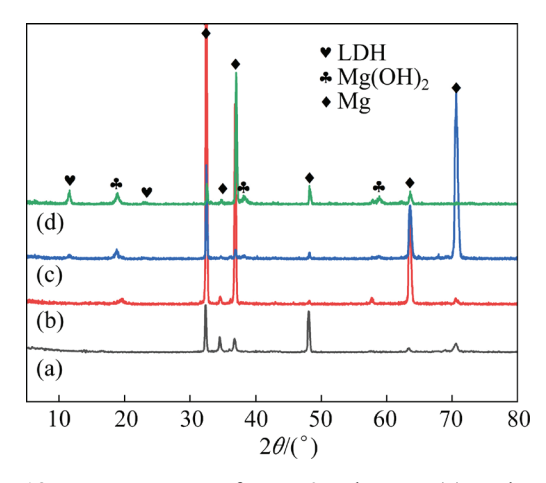


Fig. 13 XRD patterns of AM50 substrate (a) and steam coatings obtained at 0.5 h (b), 1.5 h (c) and 3 h (d)

appeared at 0.5 h, while no diffraction peaks of LDH were apparent at this stage, indicating that LDH was not formed at this time. When the reaction time reached 1.5 h, the diffraction peaks of LDH with smaller area appeared. With the reaction time extended to 3 h, there were strong

characteristic peaks of LDH at 2θ values of approximately 11.3° and 22.6° , indicating that the content of LDH increased. In addition, the diffraction peaks of Mg(OH)₂ also appeared at 18.4° , 37.9° and 58.6° .

Figure 14 displays the SEM images of the LDH coatings at reaction time of 0.5, 1.5, and 3 h, where the entire growth process of the LDH morphology on the substrate surface can be seen. When reacting for 0.5 h, the α -Mg at the edge of AlMn, Al₄Mn and β -Mg₁₇Al₁₂ phases on the surface of AM50 began to dissolve, forming Mg(OH)₂ with a network structure, and then accompanied by the continuous adsorption of Al3+. After 1.5 h reaction, Mg(OH)₂ with reticular structure grew continuously, and the generated Al3+ ions isomorphically replaced part of the Mg²⁺ ions in Mg(OH)₂ to form LDH with nanosheet structure. Under the conditions of high temperature and high pressure, OH- was supplied continuously, and LDH grew continuously like seed germination. The EDS data in Table 5

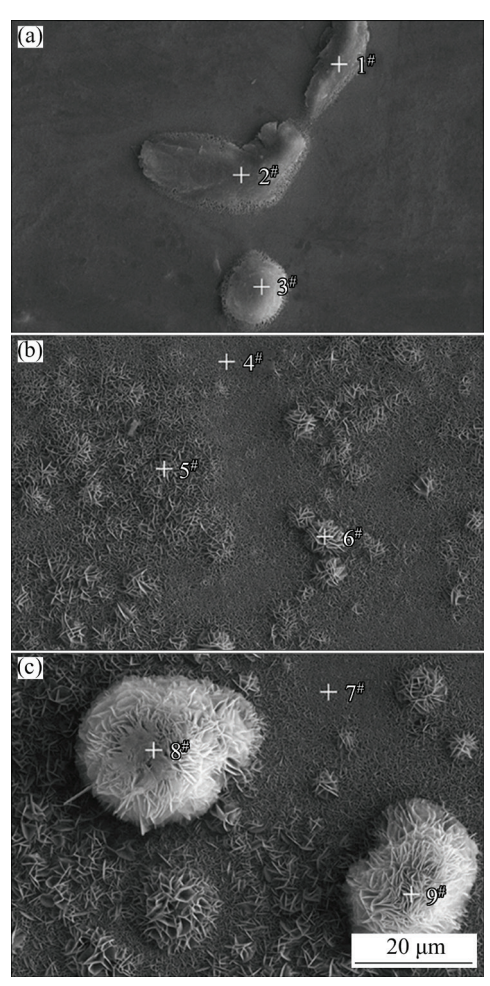


Fig. 14 SEM images of LDH coatings with reaction time of 0.5 h (a), 1.5 h (b) and 3 h (c)

Table 5 Elemental compositions of sample surface in Fig. 14 (at.%)

1 15. 1 · (a	, 0)				
Point	C	О	Mg	Al	Mn
1#	25.63	33.15	37.06	2.50	1.66
2#	23.76	44.27	20.13	6.00	5.83
3#	23.41	41.23	19.86	8.44	7.06
4#	25.62	58.34	13.88	2.16	_
5#	20.03	59.88	13.66	4.28	2.15
6#	6.17	63.49	28.69	1.62	0.03
7#	24.42	40.11	31.99	3.48	_
8#	28.11	47.24	22.88	1.78	_
9#	31.78	31.13	34.97	2.12	_

suggest that the contents of Al and Mn elements at the nucleation site of $Mg(OH)_2$ are higher (Points $4^{\#}-6^{\#}$), and it is also verified that the second phase particles are the nucleation site for the coating. After 3 h of reaction, with the continuous

deposition and adsorption of Al^{3+} , the coating continued to grow until it completely covered the whole alloy surface. Due to the continuous growth of the coating, the Mn element was covered by the growing coating, which makes manganese undetectable (Points $7^{\#}-9^{\#}$ in Table 5).

3.4.2 Effect of OA on growth mechanism of LDH coating

OA is a binary weak acid containing two carboxyl groups and has a special role in complexing with metal ions. During the growth process of the steam LDH coating, it could play an essential role in the reaction. In order to understand the effect of OA etching on the growth process of LDH coating, XPS analysis was performed on samples reacted for 0.5, 1.5 and 3 h. Figure 15 exhibits the XPS full spectra, and the C1s fine spectra of different samples. The characteristic peaks of Mg, O, C, Al, and Zn can be seen clearly from the full spectra. Figures 15(c-e) show that the C 1s spectra are composed of three peaks: C—C, 284.6 eV; C—O, 288.1 eV; C—O, 288.5 eV. The presence of C=O bonds contained in OA can be detected on the surface of the samples in the three time periods. At the reaction time of 0.5 h, the existence of C=O indicated that the OA complexed the free Mg²⁺, and Al³⁺ dissolved on the surface of the substrate, which significantly reduced the difficulty of LDH film formation. With the extension of the reaction time, the C=O bond still existed, which might be due to the formation of a water-insoluble oxalate film on the surface of AM50 at the initial stage of OA etching [41]. Therefore, the activation and complexation of OA have a significant role in the process of LDH film formation.

4 Discussion

4.1 Comparison of corrosion resistance of different LDH coatings

As the LDH coating can significantly improve the corrosion resistance of Mg alloys, our group has made extensive work in this research field. The corrosion resistance, compactness, and thickness of the LDH coatings obtained by the different preparation processes have improved to different degrees, as shown in Table 6. In terms of the preparation method, the LDH with different intercalation anions can be easily produced by the

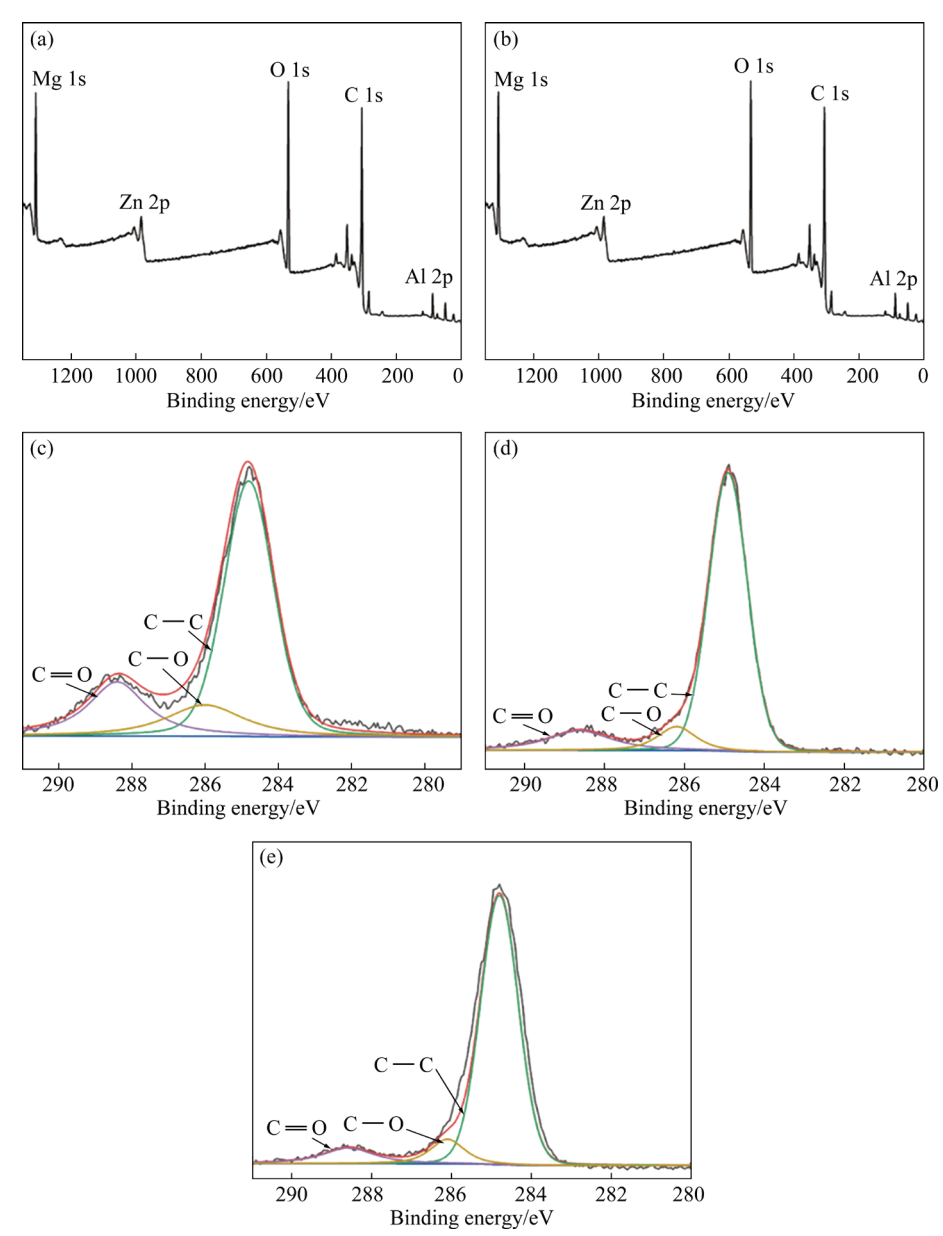


Fig. 15 XPS full spectra of coatings with reaction time of 0.5 h (a) and 3 h (b), and peaks of C 1s for coatings with reaction time of 0.5 h (c), 1.5 h (d) and 3 h (e)

Table 6 Comparison of corrosion resistance of LDH coatings based on process parameters and film thickness on different Mg alloys

	Pre-	Parameter		- Interlayer Thickness/ -		$J_{ m corr}/({ m A\cdot cm^{-2}})$			
Method	treatment	Substrate	Temperature/	Time/	ion	μm	Substrate	LDH coating	Source
Urea hydrolysis	No	AZ31	393	5	CO_3^{2-}	25-50	3.17×10^{-5}	5.75×10 ⁻⁶	[44]
Co-precipitation and hydrothermal	No	AZ31	398	36	$\mathrm{MoO_4^{2-}}$	17	3.17×10 ⁻⁵	1.60×10 ⁻⁷	[42]
Co-precipitation and hydrothermal	No	AZ31	398	36	CO_3^{2-}	7	3.04×10^{-5}	6.52×10 ⁻⁸	[43]
Steam coating	CA	AZ80	433	6	CO_3^{2-}	40.04	1.25×10^{-5}	3.58×10^{-8}	[37]
Steam coating	OA	AM50	433	6	CO_3^{2-}	61.05	2.25×10^{-5}	6.49×10^{-8}	This work

CA is citric acid

two-step co-precipitation and hydrothermal combination method [42,43]. However, the reaction time is too long and the reaction conditions are complicated. Although urea hydrolysis method [44] can be used to grow LDH on Mg alloys in one step in-situ, it can be seen from Table 6 that the prepared LDH coatings are not as corrosion-resistant as steam coatings. The LDH coatings prepared by the in-situ steam method have better adhesion to the substrate and are thicker and the coatings have better corrosion resistance. However, the trivalent cation in the LDH structure provided by the substrate limits the type and content of LDH. The acid pretreatment aims to increase the Mg-Al LDH content of the film, thus improving the corrosion resistance of the coating. The comparison of the effect of different etching acids is shown in Table 7. After CA etching, the area fraction of the second phase particles on the surface of the extruded magnesium alloy increases, which leads to the formation of a denser and thicker LDH coating [37]. OA complexes Mg²⁺ as well as Al³⁺ on the surface of Mg alloys and forms an oxalate surface film, which improves the distribution of the nucleation sites of LDH on the alloy surface. Comparing the acidity coefficients (pKa) of the two acids, we can see that pKa (OA) < pKa (CA), indicating that OA is more acidic and complex.

4.2 Schematic diagrams of formation of steam LDH coating with OA etching

Figure 16 illustrates the growth mechanism of the LDH coating on the surface of the OA-pretreated AM50, which is mainly divided into four stages.

(1) The oxide film on the surface of AM50 was dissolved when it was immersed into OA solution (Reaction (2)), and the α -Mg matrix as well as the second phase particles was exposed on the surface of AM50 alloy.

$$MgO+H_2C_2O_4=MgC_2O_4+H_2O$$
 (2)

(2) OA etching led to the dissolution of the α -Mg matrix and the release of Mg²⁺ ions, meanwhile, the intermetallic compounds including β -Mg₁₇Al₁₂ and AlMn phases released Al³⁺ ions as the pH increased. In this process, OA captured the Mg²⁺ and Al³⁺ ions, playing a certain complexing role, which increased the amount of Al³⁺ for the subsequent LDH coating growth. The corresponding reactions are as follows (Reactions (3) and (4)):

$$H_2C_2O_4+Mg=MgC_2O_4+H_2\uparrow$$
 (3)

$$3H_2C_2O_4+4Al=2Al_2(C_2O_4)_3+3H_2\uparrow$$
 (4)

(3) At 160 °C, MgO nuclei and amorphous Mg(OH)₂ began to form, and as the temperature continued to rise, MgO came into contact with the vapor to form Mg(OH)₂ with a three-dimensional network structure [46]. A steady stream of OHgathered on the surface of the alloy at high temperature and high pressure, creating an alkaline pH environment suitable for the growth of LDH. As time increased, the α -Mg phase surrounding the cathodic phase was corroded and the AlMn phase started to dissolve, reacting with water and ionizing in the higher pH environment [47]. Subsequently, Mg(OH)₂ was isomerically replaced by Al³⁺ to form LDH. The LDH coating started to nucleate and grow around the AlMn phase. The specific chemical reactions are shown as follows:

$$Mg+H_2O+2e=Mg^{2+}+2OH^-+H_2\uparrow$$
 (5)

$$Mg+2H_2O=Mg(OH)_2\downarrow+H_2\uparrow$$
 (6)

$$2A1+6H_2O=2A1(OH)_3+3H_2\uparrow$$
 (7)

(4) LDH and Mg(OH)₂ continued to grow, and finally, the steam coating completely covered the entire substrate surface.

4.3 Corrosion mechanism of LDH coatings

Figure 17 shows a schematic diagram of the corrosion mechanism of steam LDH coating on an OA pretreated AM50 Mg alloy, which is divided

Table 7 Comparison of effect of different etching acids

C144-	E4.1:	Area fraction of second phases/%		$R_{ m a}/ m \mu$	C	
Substrate	Etching acid -	Before etching	After etching	Before etching	After etching	Source
AZ31	CA	1.98 ± 0.12	5.04 ± 0.45	0.790 ± 0.01	0.950 ± 0.02	[45]
AZ80	CA	0.86 ± 0.16	2.12 ± 0.20	0.920 ± 0.02	1.310 ± 0.02	[37]
AM50	OA	0.29 ± 0.03	2.34 ± 0.29	0.075 ± 0.013	0.125±0.02	This study

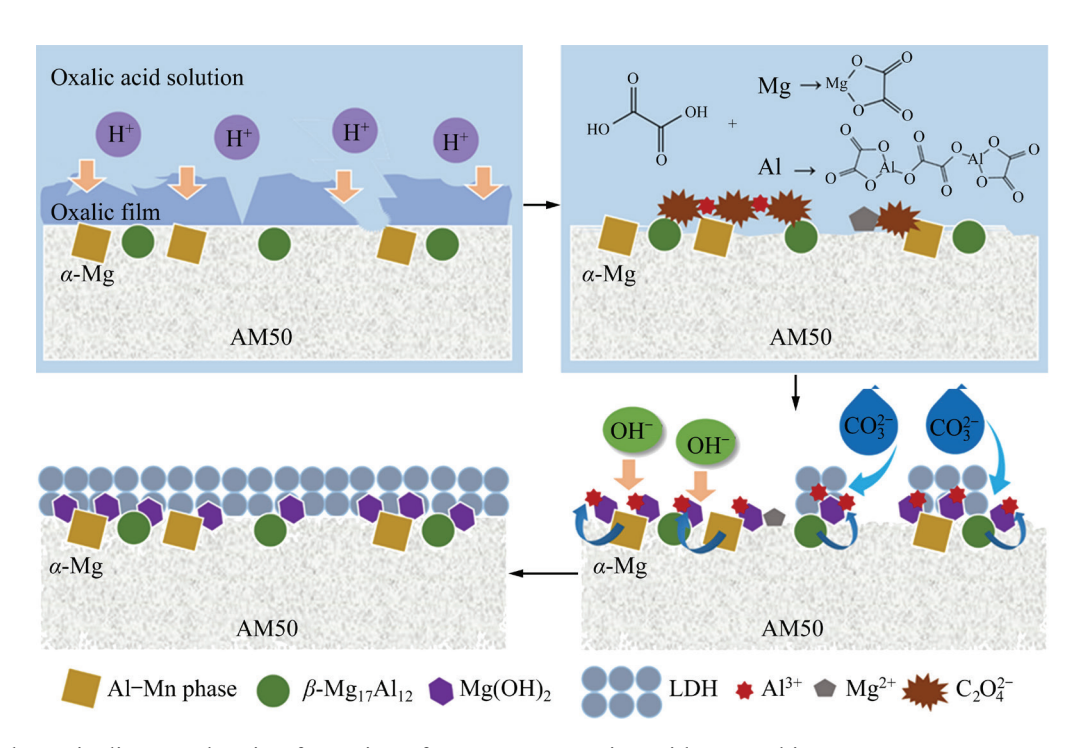


Fig. 16 Schematic diagram showing formation of steam LDH coating with OA etching

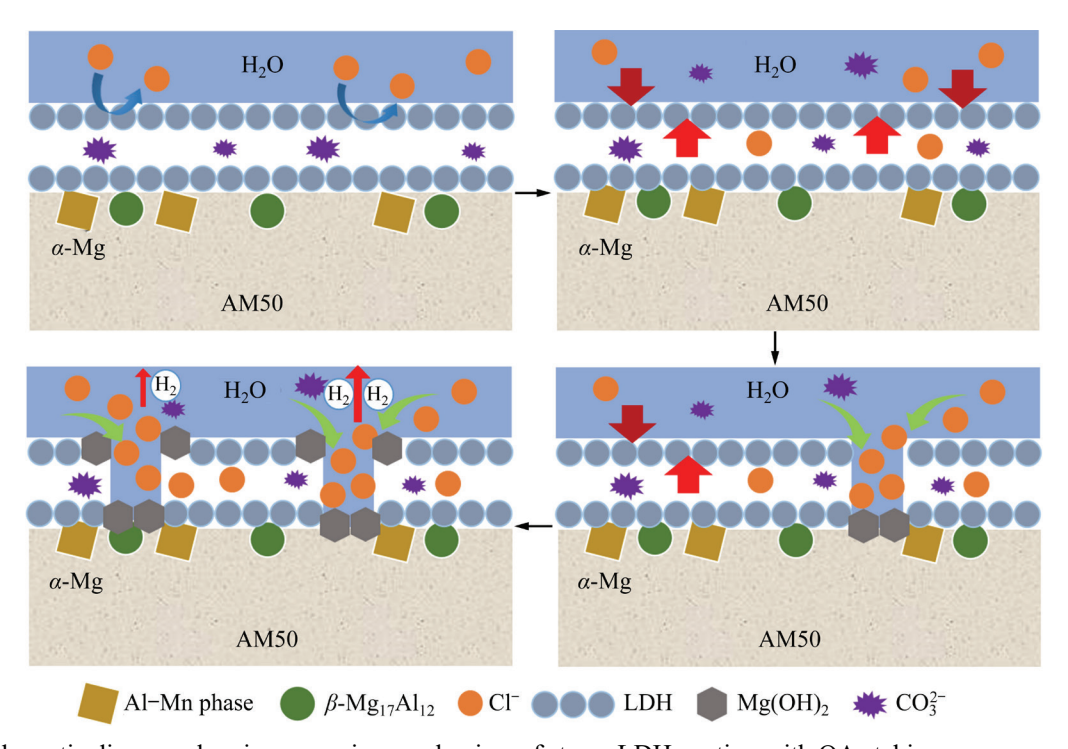


Fig. 17 Schematic diagram showing corrosion mechanism of steam LDH coating with OA etching

into the following two main stages.

(1) Under neutral salt spray conditions, the LDH in the steam coating captures the Cl⁻ in the corrosive environment through ion exchange while releasing the CO₃²⁻ ions between the laminates, achieving the first protection of the substrate through the chemical reaction of ion exchange as

well as a physical barrier. The CO₃²⁻ ions collected at the boundary of the coating and the dissolved Mg²⁺ ions in the LDH coating start to react to produce a slightly water-soluble MgCO₃ precipitate. In an alkaline environment, MgCO₃ will be transformed into Mg(OH)₂ at a faster rate, and the accumulation of corrosion products will form a

secondary protection for the substrate in a short period of time. The specific chemical reactions are shown as follows:

$$LDH - CO_3^{2-} + Cl^{-} = LDH - Cl^{-} + CO_3^{2-}$$
 (8)

$$Mg^{2+}+CO_3^{2-}=MgCO_3\downarrow$$
 (9)

$$MgCO3+2OH-=Mg(OH)2\downarrow+CO32-$$
 (10)

(2) As the physical barrier effect of the steam coating fails, the LDH—CO₃²⁻ on the surface of the sample gradually decreases. H₂O molecules and Cl⁻ ions from the steam environment gradually penetrate the coating/substrate interface through defects or pores in the coating, forming micro galvanic corrosion. Dissolution reactions occur in Mg, generating large amounts of Mg(OH)₂ and H₂ (Reaction (6)). At the same time, Cl⁻ ions can replace the OH⁻ ions in Mg(OH)₂ to form MgCl₂ (Reaction (11)), which has a high solubility in water. Finally, damage and failure of the coating are caused by the volume expansion of the corrosion products and the upward force exerted by H₂.

$$Mg(OH)_2+2Cl^-=MgCl_2+2OH^-$$
 (11)

5 Conclusions

- (1) Mg-Al LDH coatings grew on AM50 alloys via an in-situ rapid steam coating method combined with an organic acid OA pretreatment. As compared with the polished AM50 substrate, the area fraction of the second phase was increased by approximately 7 times.
- (2) The OA etching of AM50 Mg alloy significantly enhanced the corrosion resistance of in-situ steam LDH coatings. The corrosion current density of OA/LDH-45s sample (J_{corr} = 6.49×10^{-8} A/cm²) was two orders of magnitude lower than that of the LDH coatings without OA etching (J_{corr} =1.55×10⁻⁶ A/cm²). Also, the salt spray test demonstrated excellent corrosion protection of the OA/LDH-45s samples.
- (3) The α -Mg matrix in AM50 Mg alloy was etched preferentially and the second phases including AlMn and β -Mg₁₇Al₁₂ retained during acid etching, which provided the nucleation sites for the subsequent formation of LDH coating. Furthermore, OA complexed Mg²⁺ and Al³⁺ ions on the surface of AM50 Mg alloy to form water-insoluble oxalates, and this film layer can effectively improve the distribution of Al species

and is useful for the growth of LDH coating.

(4) The OA etching is a beneficial process for solving the problem of insufficient Al source and inhomogeneous composition in the growth process of steam LDH coating on Mg alloys.

CRediT authorship contribution statement

Shi-qi PAN: Investigation, Formal analysis, Data curation, Writing - Original draft; Jin-meng WANG: Conceptualization, Methodology, Software; Fen ZHANG: Investigation, Funding acquisition, Resources, Supervision, Writing – Review & editing; Hao-feng XIE: Resources, Supervision; Lan-yue CUI: Software, Validation; M. BOBBY KANNAN: Writing – Review & editing; Yu-hong ZOU: Funding acquisition, Supervision; **ZENG:** Conceptualization, Rong-chang Funding acquisition, Resources, Supervision, Writing - Review & editing.

Declaration of competing interest

The authors declare that they have no known competing financial interests or personal relationships that might influence the work reported here.

Acknowledgments

This work was supported by the National Natural Science Foundation of China (Nos. 51601108, 52071191) and the Natural Science Foundation of Shandong Province, China (No. ZR2020ME011).

References

- [1] ZHAO Chen, CAO Fu-yong, SONG Guang-ling. Corrosivity of haze constituents to pure Mg [J]. Journal of Magnesium and Alloys, 2020, 8(1):150–162.
- [2] CHENG Yuan-fen, DU Wen-bo, LIU Ke, FU Jun-jian, WANG Zhao-hui, LI Shu-bo, FU Jin-long. Mechanical properties and corrosion behaviors of Mg-4Zn-0.2Mn-0.2Ca alloy after long term in vitro degradation [J]. Transactions of Nonferrous Metals Society of China, 2020, 30(2): 363-372.
- [3] LI Chuan-qiang, TONG Zhi-pei, HE Yi-bin, HUANG Huai-pei, DONG Yong, ZHANG Peng. Comparison on corrosion resistance and surface film of pure Mg and Mg-14Li alloy [J]. Transactions of Nonferrous Metals Society of China, 2020, 30(9): 2413–2423.
- [4] ZHAO Xia, WEI Jin-fei, LI Bu-cheng, LI Si-bei, TIAN Ning, JING Ling-yun, ZHANG Jun-ping. A self-healing superamphiphobic coating for efficient corrosion protection of magnesium alloy [J]. Journal of Colloid and Interface Science, 2020, 575: 140–149.
- [5] WANG Dan-qian, PEI San-le, WANG Ye, MA Kai, DAI, Chao-neng, WANG Jin-xing, WANG Jing-feng, PAN,

- Fu-sheng. Effect of magnesium-to-phosphate ratio on the corrosion resistance of magnesium alloy embedded in magnesium potassium phosphate cement [J]. Cement and Concrete Composites, 2023, 135: 104826.
- [6] PRASAD A, VASHISHTHA H, SINGH S S, GOSVAMI N N, JAIN, J K. La containing Mg alloy for enhanced corrosion at elevated temperatures in ethylene glycol media [J]. Corrosion Science, 2022, 205: 110446.
- [7] SHIRI M, JAFARI H, SINGH R. Effect of extrusion parameters on degradation of magnesium alloys for bioimplant applications: A review [J]. Transactions of Nonferrous Metals Society of China, 2022, 32(9): 2787–2813.
- [8] YUAN Bo, CHEN He-wei, ZHAO Rui, DENG Xuan-geng, CHEN Guo, YANG Xiao, XIAO Zhan-wen, AURORA A, IULIA B A, ZHNG Kai, ZHU Xiang-dong, IULIAN A V, HAI Shen, ZHANG Xing-dong. Construction of a magnesium hydroxide/graphene oxide/hydroxyapatite composite coating on Mg-Ca-Zn-Ag alloy to inhibit bacterial infection and promote bone regeneration [J]. Bioactive Materials, 2022, 18: 354-367.
- [9] CAI Lei, MEI Di, ZHANG Zhao-qi, HUANG Yuan-ding, CUI Lan-yue, GUAN Shao-kang, CHEN Dong-chu, KANNAN M B, ZHENG Yu-feng, ZENG Rong-chang. Advances in bioorganic molecules inspired degradation and surface modifications on Mg and its alloys [J]. Journal of Magnesium and Alloys, 2022, 10(3): 670–688.
- [10] YADAV V S, SANKAR M R, PANDEY L M. Coating of bioactive glass on magnesium alloys to improve its degradation behavior: Interfacial aspects [J]. Journal of Magnesium and Alloys, 2020, 8(4): 999–1015.
- [11] PENG Feng, ZHANG Dong-dong, LIU Xuan-yong, ZHANG Yu. Recent progress in superhydrophobic coating on Mg alloys: A general review [J]. Journal of Magnesium and Alloys, 2021, 9(5): 1471–1486.
- [12] MENG Xue, WANG Jin-lei, ZHANG Jie, NIU Bao-long, GAO Xiang-hua, YAN Hong. Electroplated superhydrophobic Zn–Fe coating for corrosion protection on magnesium alloy [J]. Transactions of Nonferrous Metals Society of China, 2022, 32(10): 3250–3258.
- [13] GAO Ju-lia, SU Ying-chao, QIN Yi-xian. Calcium phosphate coatings enhance biocompatibility and degradation resistance of magnesium alloy: Correlating in vitro and in vivo studies [J]. Bioactive Materials, 2021, 6(5): 1223-1229.
- [14] ZHAO Yan-bin, CHEN Xue-yang, LI Shuo-qi, ZENG Rong-chang, ZHANG Fen, WANG Zhen-lin, GUAN Shao-kang. Corrosion resistance and drug release profile of gentamicin-loaded polyelectrolyte multilayers on magnesium alloys: Effects of heat treatment [J]. Journal of Colloid and Interface Science, 2019, 547: 309–317.
- [15] LIU Yan, XUE Jing-ze, LUO Dan, WANG Hui-yuan, GONG Xu, HAN Zhi-wu, REN Lu-quan. One-step fabrication of biomimetic superhydrophobic surface by electrodeposition on magnesium alloy and its corrosion inhibition [J]. Journal of Colloid and Interface Science, 2017, 491: 313–320.
- [16] SANKARA N T S N, PARK I S, LEE M H. Strategies to

- improve the corrosion resistance of microarc oxidation (MAO) coated magnesium alloys for degradable implants: Prospects and challenges [J]. Progress in Materials Science, 2014, 60: 1–71.
- [17] YAO Wen-hui, WU Liang, WANG Jing-feng, JIANG Bin, ZHANG Ding-fei, SERDECHNOVA M, SHULHA T, BLAWERT C, ZHELUDKEVICH M L, PAN Fu-sheng. Micro-arc oxidation of magnesium alloys: A review [J]. Journal of Materials Science & Technology, 2022, 118: 158–180.
- [18] JIANG Dan, XIA Xian-chao, HOU Jian, CAI Guang-yi, ZHANG Xin-xin, DONG Ze-hua. A novel coating system with self-reparable slippery surface and active corrosion inhibition for reliable protection of Mg alloy [J]. Chemical Engineering Journal, 2019, 373: 285–297.
- [19] WANG Xin, JING Chuan, CHEN Yu-xiang, WANG Xiu-shuang, ZHAO Gang, ZHANG Xing, WU Liang, LIU Xiao-ying, DONG Bi-qin, ZHANG Yu-xin. Active corrosion protection of super-hydrophobic corrosion inhibitor intercalated Mg-Al layered double hydroxide coating on AZ31 magnesium alloy [J]. Journal of Magnesium and Alloys, 2020, 8(1): 291–300.
- [20] CHEN Yan-ning, WU Liang, YAO Wen-hui, WU Jia-hao, XIANG Jian-peng, DAI Xiao-wei, WU Tao, YUAN Yuan, WANG Jing-feng, JIANG Bin, PAN Fu-sheng. Development of metal-organic framework (MOF) decorated graphene oxide/MgAl-layered double hydroxide coating via microstructural optimization for anti-corrosion micro-arc oxidation coatings of magnesium alloy [J]. Journal of Materials Science & Technology, 2022, 130: 12–26.
- [21] KWON D, KANG J Y, AN S, YANG I, JUNG J C. Tuning the base properties of Mg-Al hydrotalcite catalysts using their memory effect [J]. Journal of Energy Chemistry, 2020, 46: 229-236.
- [22] NIETO Z S, RAMOS R E, TZOMPANTZI M F, BOFFITO D C, NACCACHE R, GUTIEERRZ O N L, LITTER M I, CIPAGAUTA D S, BARBOSA L A L. ZnAl hydrotalcites modified with nanocomposites nZVI–PAA for environmental remediation [J]. Journal of Materials Research and Technology, 2021, 14: 2243–2256.
- [23] ALZEER M I M, NGUYEN H, FABRITIUS T, SREENIVASAN H, TELKKI V V, KANTOLA A M, CHEESEMAN C, ILLIKAINEN M, KINNUNEN P. On the hydration of synthetic aluminosilicate glass as a sole cement precursor [J]. Cement and Concrete Research, 2022, 159: 106859.
- [24] ISHIZAKI T, CHIBA S, WATANABE K, SUZUKI H. Corrosion resistance of Mg-Al layered double hydroxide container-containing magnesium hydroxide films formed directly on magnesium alloy by chemical-free steam coating [J]. Journal of Materials Chemistry A, 2013, 1(31): 8968-8977.
- [25] KAMIYAMA N, PANOMSUWAN G, YAMAMOTO E, SUDARE T, SAITO N, ISHIZAKI T. Effect of treatment time in the Mg(OH)₂/Mg-Al LDH composite film formed on Mg alloy AZ31 by steam coating on the corrosion resistance

- [J]. Surface and Coatings Technology, 2016, 286: 172-177.
- [26] YIN Ming, HOU Li-feng, WANG Zhi-wei, BAO Tong-yao, LIU Bao-sheng, WEI Huan, LIU Xiao-da, DU Hua-yun, WEI Ying-hui. Self-generating construction of applicable corrosion-resistant surface structure of magnesium alloy [J]. Corrosion Science, 2021, 184: 109378.
- [27] MORENO J, MERLO J L, RENNO A C, CANIZO J, BUCHELLY F J, PASTORE J I, KATUNAR M R, CERE S. In vitro characterization of anodized magnesium alloy as a potential biodegradable material for biomedical applications [J]. Electrochimica Acta, 2023, 437: 141463.
- [28] CAO Fu-yong, SONG Guang-ling, ATRENS A. Corrosion and passivation of magnesium alloys [J]. Corrosion Science, 2016, 111: 835–845.
- [29] ZHANG Dong-dong, PENG Feng, TAN Ji, LIU Xuan-yong. In-situ growth of layered double hydroxide films on biomedical magnesium alloy by transforming metal oxyhydroxide [J]. Applied Surface Science, 2019, 496: 143690.
- [30] ISHIZAKI T, MIYASHITA T, INAMURA M, NAGA-SHIMA Y, SERIZAWA A. Effect of Al content in the Mg-based alloys on the composition and corrosion resistance of composite hydroxide films formed by steam coating [J]. Materials, 2019, 12(7): 1188.
- [31] CHEN X B, BIRBILIS N, ABBOTT T. B. Review of corrosion-resistant conversion coatings for magnesium and its alloys [J]. Corrosion, 2011, 67(3): 035005.
- [32] YANG Hai-yan, CHEN Xiao-bo, GUO Xing-wu, WU Guo-hua, DING Wen-jiang, BIRBILIS N. Coating pretreatment for Mg alloy AZ91D [J]. Applied Surface Science, 2012, 258(14): 5472-5481.
- [33] SHAO Zhong-cai, CAI Zhi-qiang, HU Rong, WEI Shou-qiang. The study of electroless nickel plating directly on magnesium alloy [J]. Surface and Coatings Technology, 2014, 249: 42–47.
- [34] TAN J K E, BIRBILIS N, CHOUDHARY S, CHOUDHARY S, THOMAS S, BALAN P. Corrosion protection enhancement of Mg alloy WE43 by in-situ synthesis of MgFe LDH/citric acid composite coating intercalated with 8HQ [J]. Corrosion Science, 2022, 205: 110444.
- [35] LIU Qun, PAN Dan, DING Ting-ting, YE Meng-chao, HE Feng-jiao. Clean & environmentally friendly regeneration of Fe-surface cleaning pickling solutions [J]. Green Chemistry, 2020, 22(24): 8728–8733.
- [36] ARTHANARI S, NALLAIYAN R, KWANG S S. Electrochemical corrosion behavior of acid treated strip cast AM50 and AZX310 magnesium alloys in 3.5 wt.% NaCl solution [J]. Journal of Magnesium and Alloys, 2017, 5(3): 277–285.
- [37] WANG Jin-meng, SUN Xiang, SONG Liang, KANNAN M. B, ZHANG Fen, CUI Lan-yue, ZOU Yu-hong, LI Shuo-qi, ZENG Rong-chang. Corrosion resistance of Mg-Al-LDH steam coating on AZ80 Mg alloy: Effects of citric acid

- pretreatment and intermetallic compounds [J]. Journal of Magnesium and Alloys, 2023, 11: 2967–2979.
- [38] LI Nan, LI Qing, GUO Xiao-tian, YUAN Mei-juan, PANG Huan. Controllable synthesis of oxalate and oxalate-derived nanomaterials for applications in electrochemistry [J]. Chemical Engineering Journal, 2019, 372: 551–571.
- [39] CHEN Hai-yang, REN Bo, LIU Meng, QIN Ting-wei, GUO Qiang, LI Guang-qi, GONG Dian-sheng, CHENG Guang-lin, CHEN Jun-hong, LI Bin. Facile synthesis of hydroxyl aluminum oxalate based on the hydrothermal reaction of boehmite and oxalic acid [J]. Colloids and Surfaces A: Physicochemical and Engineering Aspects, 2022, 639: 128344
- [40] NWAOGU U C, BLAWERT C, SCHARNAGL N, DIETZEL W, KAINER K U. Effects of organic acid pickling on the corrosion resistance of magnesium alloy AZ31 sheet [J]. Corrosion Science, 2009, 52: 2143–2154.
- [41] JIANG Yong-feng, ZHOU Hai-tao, ZENG Su-min. Microstructure and properties of oxalate conversion coating on AZ91D magnesium alloy [J]. Transactions of Nonferrous Metals Society of China, 2009, 19(6): 1416–1422.
- [42] ZENG Rong-chang, LI Xiao-ting, LIU Zhen-guo, ZHANG Fen, LI Shuo-qi, CUI Hong-zhi. Corrosion resistance of Zn-Al layered double hydroxide/poly(lactic acid) composite coating on magnesium alloy AZ31 [J]. Frontiers of Materials Science, 2015, 9(4): 355–365.
- [43] ZHANG Fen, LIU Zhen-guo, ZENG Rong-chang, LI Shuo-qi, CUI Hong-zhi, SONG Liang, HAN En-hou. Corrosion resistance of Mg-Al-LDH coating on magnesium alloy AZ31 [J]. Surface and Coatings Technology, 2014, 258: 1152-1158.
- [44] ZENG Rong-chang, LIU Zhen-guo, ZHANG Fen, LI Shuo-qi, HE Qing-kun, CUI Hong-zhi, HAN En-hou. Corrosion resistance of in-situ Mg-Al hydrotalcite conversion film on AZ31 magnesium alloy by one-step formation [J]. Transactions of Nonferrous Metals Society of China, 2015, 25(6): 1917-1925.
- [45] LI Feng, SUN Xiang, SONG Liang, KANNAN M B, ZHANG Fen, CUI Lan-yue, ZOU Yu-hong, LI Shuo-qi, LIU Cheng-bao, ZENG Rong-chang. Influence of intermetallic Al-Mn particles on in-situ steam Mg-Al-LDH coating on AZ31 magnesium alloy [J]. Transactions of Nonferrous Metals Society of China, 2022, 32(12): 3926–3949.
- [46] NAKAMURA K, TSUNAKAWA M, SHIMADA Y, SERIZAWA A, ISHIZAKI T. Formation mechanism of Mg-Al layered double hydroxide-containing magnesium hydroxide films prepared on Ca-added flame-resistant magnesium alloy by steam coating [J]. Surface and Coatings Technology, 2017, 328: 436-443.
- [47] ZENG Rong-chang, ZHANG Fen, LAN Zi-dong, CUI Hongzhi, HAN En-hou. Corrosion resistance of calcium-modified zinc phosphate conversion coatings on magnesium aluminium alloys [J]. Corrosion Science, 2014, 88: 452–459.

草酸预处理 AM50 镁合金表面快速原位制备蒸汽 Mg-Al LDH 涂层的耐蚀性

潘仕琪¹, 王金梦¹, 张 芬¹, 解浩峰², 崔蓝月¹, M. BOBBY KANNAN³, 邹玉红⁴, 曾荣昌^{1,5}

- 1. 山东科技大学 材料科学与工程学院 轻金属腐蚀实验室, 青岛 266590;
- 2. 有研工程技术研究院有限公司 有色金属材料制备加工国家重点实验室, 北京 100088;
- 3. School of Engineering, University of Newcastle, Callaghan, New South Wales, 2308, Australia;
 - 4. 山东科技大学 化学与环境工程学院, 青岛 266590;
 - 5. 郑州大学 材料科学与工程学院,郑州 450002

摘 要:通过暴露合金表面的金属间化合物(β-Mg₁₇Al₁₂和 AlMn),研究草酸(OA)酸洗对 AM50 镁合金表面原位蒸汽 Mg-Al 层状双氢氧化物(LDH)涂层成膜机制和耐蚀性的影响。结果表明,OA 预处理使镁合金表面金属间化合物比例显著增加,Mg-Al LDH 在 Al-Mn 相周围成核并生长。当酸洗时间为 45 s 时,所得 LDH 涂层的厚度最大、耐蚀性最佳,与基体相比,其腐蚀电流密度降低 3 个数量级。最后,提出了 AM50 镁合金表面 Mg-Al LDH 涂层的成膜机制。

关键词: 镁合金; 草酸; 金属间化合物; 蒸汽涂层; 层状双氢氧化物; 耐蚀性

(Edited by Wei-ping CHEN)